Journal of Anatomy

J. Anat. (2015) **227**, pp596–610 doi: 10.1111/joa.12368

Scar-free cutaneous wound healing in the leopard gecko, *Eublepharis macularius*

Hanna M. Peacock,† Emily A. B. Gilbert and Matthew K. Vickaryous

Department of Biomedical Sciences, Ontario Veterinary College, University of Guelph, Guelph, ON, Canada

Abstract

Cutaneous wounds heal with two possible outcomes: scarification or near-perfect integumentary restoration. Whereas scar formation has been intensively investigated, less is known about the tissue-level events characterising wounds that spontaneously heal scar-free, particularly in non-foetal amniotes. Here, a spatiotemporal investigation of scar-free cutaneous wound healing following full-thickness excisional biopsies to the tail and body of leopard geckos (*Eublepharis macularius*) is provided. All injuries healed without scarring. Cutaneous repair involves the development of a cell-rich aggregate within the wound bed, similar to scarring wounds. Unlike scar formation, scar-free healing involves a more rapid closure of the wound epithelium, and a delay in blood vessel development and collagen deposition within the wound bed. It was found that, while granulation tissue of scarring wounds is hypervascular, scar-free wound healing conspicuously does not involve a period of exuberant blood vessel formation. In addition, during scar-free wound healing the newly formed blood vessels are typically perivascular cell-supported. Immunohistochemistry revealed widespread expression of both the pro-angiogenic factor vascular endothelial growth factor A and the anti-angiogenic factor thrombospondin-1 within the healing wound. It was found that scar-free wound healing is an intrinsic property of leopard gecko integument, and involves a modulation of the cutaneous scar repair program. This proportional revascularisation is an important factor in scar-free wound healing.

Key words: biopsy punch; blood vessels; collagen; *Eublepharis macularius*; histology; PCNA; perivascular cells; TSP-1; VEGF; wound epithelium.

Introduction

Cutaneous wound healing is an essential process for maintaining skin integrity and homeostasis. Skin forms the primary interface between the external environment and the body, participating as a structural barrier in preventing water loss and impeding pathogen entry; it also plays an important role in thermoregulation and somatosensation (Baum & Arpey, 2005; Ross & Pawlina, 2011). Disruption of the integument can seriously impair these functions, and thus requires a rapid restorative response to ensure survival (Clark et al. 2007; Yates et al. 2013). In mammals, cutaneous repair typically involves fibrosis, the abnormal deposition of collagen to form scar tissue. Cutaneous scars are permanent, injury-mediated disruptions of the normal skin architecture (Ferguson et al. 1996). While scarring does restore the barrier between the body and the external environment, it is a dysfunctional and disfiguring solution (Occleston et al. 2010). In mammals, cutaneous scars lack hair follicles and sweat glands, and hence are unable to contribute to thermoregulation (Driskell et al. 2013). Fully mature scar tissue also differs structurally from uninjured skin in the arrangement of dermal collagen (parallel bundles rather than basket-weave) and in the absence of elastin. Consequently, scarred skin has only 80% of the tensile strength of the original (undamaged) organ (Levenson et al. 1965; Occleston et al. 2010).

Scar formation is characterised by an overlapping cascade of tissue events beginning with haemostasis and inflammation. This is followed by re-establishment of the epidermis, fibroblast proliferation, and extensive angiogenesis and collagen deposition (Gurtner et al. 2008). Haemostasis is achieved by rapid and localised vasoconstriction and the formation of a fibrin clot (Guo & DiPietro, 2010; Reinke & Sorg, 2012). Concurrently, inflammation is initiated by platelet degranulation and the expression of pro-inflamma-

Correspondence
Matthew K. Vickaryous, Associate Professor, Department of Biomedical Science, University of Guelph, 50 Stone Road East, Guelph, ON, Canada N1G 2W1. T: 1-519-760-2374 x 53871; E: mvickary@uoguelph.ca

†*Present address: Department of Cardiovascular Sciences, KU Leuven, Leuven, Belgium*

Accepted for publication *17 July 2015*
Article published online *11 September 2015*

tory cytokines (Reinke & Sorg, 2012). Restoration of the epidermis begins as keratinocytes migrate beneath the fibrin clot to form the wound epithelium (Gurtner et al. 2008). Fibroblasts from the uninjured dermis migrate into the wound defect, proliferate, and begin depositing a provisional extracellular matrix (ECM; Satish & Kathju, 2010). Subsets of these (and possibly other) cells differentiate into contractile cells, known as myofibroblasts, which bring the wound edges closer together and deposit large amounts of collagen (Greaves et al. 2013). Blood vessels sprout vigorously into the wound bed such that the vascular density of the newly forming tissue greatly exceeds that of the normal dermis (Bluff et al. 2006; Dipietro, 2013). This highly vascular, highly cellular aggregation, granulation tissue, is ultimately remodelled to form the final hypovascular, hypocellular scar (Satish & Kathju, 2010). The remodelling process involves resolution of inflammation, extensive vascular regression through apoptosis of endothelial cells, and restructuring of the scar ECM into parallel bundles of collagen (Epstein et al. 1999).

While scarification is the most familiar mode of wound healing, some vertebrates are capable of near-perfect skin restoration. Many of the best understood examples come from amphibians, including axolotls (*Ambystoma mexicanum*; Lévesque et al. 2010; Seifert et al. 2012) and premetamorphic frogs (i.e. tadpoles; Yannas et al. 1996; Yokoyama et al. 2011; Bertolotti et al. 2013). Among various mammalian species, including mice and humans, the foetus is capable of scar-free cutaneous wound healing until early- to mid-gestation (Lorenz et al. 1992; Ferguson & O'Kane, 2004). Beyond this time, injuries to the skin, as for most other organs of the body, scar. Although scar-free cutaneous wound healing by adult mammals is rare, it has been documented in African spiny mice (*Acomys kempi* and *A. percivali*; Seifert et al. 2013) and the mutant PU.1 null mouse strain, which lacks macrophages (Martin et al. 2003). Similarly, some lizard species (e.g. the gekkotans *Hemidactylus* and *Tarentola*; the dactyloid *Anolis*) are also capable of scar-free wound healing, as evidenced by the restoration of scales following cutaneous injury (Woodland, 1920; Noble & Bradley, 1933; Wu et al. 2014).

To date, investigations of scar-free wound healing have mainly focused on two early, interconnected events: inflammation and re-epithelialisation (Lévesque et al. 2010; Satish & Kathju, 2010; Seifert et al. 2012, 2013). These studies indicate that, while the initial sequence of tissue-level events during scar-free wound healing closely parallels those of scar formation, there are some obvious differences. For example, the inflammatory phase of scar formation is characterised by the infiltration of large numbers of neutrophils as well as the expression of pro-inflammatory cytokines (e.g. TGF-β1 and 2, PDGF, IL-1, IL-6 and TNF-α; Barrientos et al. 2008). In contrast, during scar-free wound healing the inflammatory phase involves only a limited number of neutrophils and increased expression of anti-inflammatory cytokines (e.g. IL-10 and TGF-β3; Lévesque et al. 2010; Satish & Kathju, 2010; Seifert et al. 2012). Another difference involves the rate of re-epithelialisation. In scar-forming adult mice, 4–6 mm in diameter excisional wounds take 6–14 days post-wounding (DPW) to re-epithelialise (Galiano et al. 2004; Lucas et al. 2010; Chen et al. 2014), whereas adult axolotls close similarly-sized wounds in as few as 18 h during scar-free healing (Seifert et al. 2012). However, little is known about the events that occur during scar-free wound healing after re-epithelialisation has taken place.

Here, the tissue events characteristic of scar-free cutaneous wound healing in the leopard gecko, *Eublepharis macularius* (Blyth, 1854), were investigated. Leopard geckos offer several advantages as representative lizard models for laboratory investigations, including that they have a relatively conservative 'lizard' body plan (e.g. eyelids are present, subdigital adhesive pads are absent, no evidence of digit loss or trunk elongation) and occupy a basal phylogenetic position among Squamata (lizards + snakes; Pyron et al. 2013). They are also commercially captive bred and widely available in the pet trade, are tolerant of handling and experimental manipulations (e.g. anaesthesia, tail amputation), and have comparatively simple husbandry requirements (see Materials and methods; McLean & Vickaryous, 2011; Delorme et al. 2012). In addition, as for many lizards (Alibardi, 2010), they are capable of self-detaching (autotomising) the tail (to escape predation) and then spontaneously regenerating a replacement (McLean & Vickaryous, 2011; Delorme et al. 2012). The regenerative capacity of the leopard gecko was explored, focusing on the skin of both the body and tail using 3-mm-diameter full-thickness biopsy wounds. It was determined that leopard geckos spontaneously heal cutaneous excisional wounds without fibrosis. Re-epithelialisation occurs within 5 DPW, concurrent with proliferation of fibroblast-like cells. Compared with reports of scar formation, it was found that the onset of blood vessel formation within the wound bed is delayed (5–8 DPW in leopard geckos vs. 2–3 DPW reported for mammals). Unlike scar formation, the wound bed showed no evidence of excessive vasculature during scar-free wound healing. Blood vessels that were present rapidly became structurally mature.

Materials and methods

Animal care

Captive bred juvenile *E. macularius* were obtained from a commercial supplier (Global Exotic Pets, Kitchener, Ontario, Canada). At the beginning of the trial, all leopard geckos were subadults (< 1 year old and not sexually mature) and had an average mass of 10.8 g (range: 7.8–17.6 g; see Data S1). Animal Usage Protocols were approved by the University of Guelph Animal Care Committee (Protocol Number 2493), and followed the policies and procedures of the Canadian Council on Animal Care. Animal husbandry followed the protocols of Vickaryous & McLean (2011). Briefly, leopard

geckos were housed individually in 5-gallon plastic tanks in an isolated environmental chamber with a 12 : 12 photoperiod, and average ambient temperature of 27.5 °C. A temperature gradient was created beneath the tanks using a subsurface heating cable (Hagen, Baie d'Urfé, Québec, Canada) under one end of the enclosure set to 32 °C. Animals were fed a daily diet of gut-loaded mealworms (larval *Tenebrio* spp.) dusted with a powdered calcium and vitamin D3 (cholecalciferol) supplement (Zoo Med Laboratories, San Luis Obispo, CA, USA). Experimental observations of wound healing involved a total of 35 individuals (Data S1). Seven additional individuals were used as environmental controls (i.e. sentinels) throughout the experiment, and were monitored for growth and weight gain, but otherwise were unmanipulated (Data S1).

Biopsies

Leopard geckos were anaesthetised by intramuscular injection of 30 mg kg^{-1} Alfaxan (diluted to 2 mg mL^{-1} in sterile injectable 0.9% sodium chloride, using a 0.5 cc insulin syringe; Abbott Laboratories, Saint-Laurent, Québec, Canada) bilaterally, as a divided dose, into epaxial muscles of the neck. The surgical plane of anaesthesia was established when leopard geckos no longer exhibited a righting reflex (Schumacher & Yelen, 2006). Once surgical anaesthesia was achieved, full-thickness excisional cutaneous wounds were created using a 3-mm disposable biopsy tool (Integra Miltex, Burlington, Ontario, Canada). Each biopsy was centred on a single tubercle scale, and the depth of the excision was adjusted to interrupt the epidermis, dermis and part of the hypodermis. The tissue plug was removed using forceps and a #11 scalpel blade. Each animal received two dorsally located biopsies: one on the body wall and one on the distal portion of the original tail (Fig. 1).

Tissue collection

After receiving the full-thickness excisional biopsies, animals were permitted to heal. At select time points (corresponding to 0.5, 2, 5, 8, 14, 28 and 45 DPW; Fig. S1), leopard geckos were humanely killed using an intra-abdominal injection of 250–500 mg tricaine methansulphonate (MS222). Tissues were then fixed [either by transcardial perfusion of the whole animal with saline followed by 10% neutral buffered formalin (NBF) followed by immersion in 10% NBF for 24 h, or by dissection of tissues of interest followed by direct immersion in 10% NBF for 24 h] and stored in 70% ethanol. Before processing, tissues were decalcified in Cal-Ex™ (Fischer Scientific, Waltham, MA, USA) for 30 min. Tissues of interest were then dehydrated to 100% isopropanol, cleared in xylene and embedded in paraffin wax (Fischer Scientific). Sections were cut at 5 μm on a rotary microtome, mounted on charged slides (Surgipath® X-tra®; Leica Microsystems, Concord, Ontario, Canada), and baked at 37 °C overnight.

Masson's trichrome

To differentiate fibrous tissue, representative sections were stained using a modified Masson's trichrome (McLean & Vickaryous, 2011). Briefly, slides were rehydrated to water: three (2 min) changes each of xylene and then absolute isopropanol, and one (2 min) change in 70% isopropanol followed by (2 min) deionised water. Slides were stained (10 min) with Mayer's haematoxylin, rinsed in deionised water, blued in ammonia water (~15 s), and rinsed in deionised water again. Slides were then stained (2 min) in 0.5% ponceau xylidine/0.5% acid fuchsin in 1% acetic acid solution and rinsed in deionised water. Slides were then incubated (10 min) in 1% phosphomolybdic acid and rinsed in deionised water before being stained (90 s) in 2% light green, and rinsed again in deionised water. Slides were then dehydrated through 95% isopropanol (2 min) followed by three (2 min) changes each of absolute isopropanol and xylene. Slides were coverslipped using Cytoseal (TM) (Fischer Scientific).

Immunohistochemistry

To visualise expression of the proteins WE6, proliferating cell nuclear antigen (PCNA), vascular endothelial growth factor (VEGF) and thrombospondin-1 (TSP-1) adjacent to and within the wound bed, immunohistochemistry was performed. Slides were baked overnight at 60 °C and then rehydrated to water (as above). Sections were quenched for 20 min in 3% hydrogen peroxide. Slides were then rinsed with three (2 min) changes in phosphate-buffered saline (PBS). For each of WE6, VEGF and TSP-1, heat-induced antigen retrieval was performed (citrate buffer at 90 °C for 12 min, and allowed to cool in the buffer for 20 min). Slides were then rinsed with three (2 min) changes of PBS. Sections were then blocked using 3% normal goat serum (NGS; Vector Laboratories, Burlingame, CA, USA) diluted in PBS for either 1 h (VEGF, TSP-1, PCNA) or 90 min (WE6) at room temperature. Sections were then incubated overnight at 4 °C with primary antibody diluted in PBS (for details and specific dilutions, see Table 1) or, for the negative control sections, PBS. Slides were

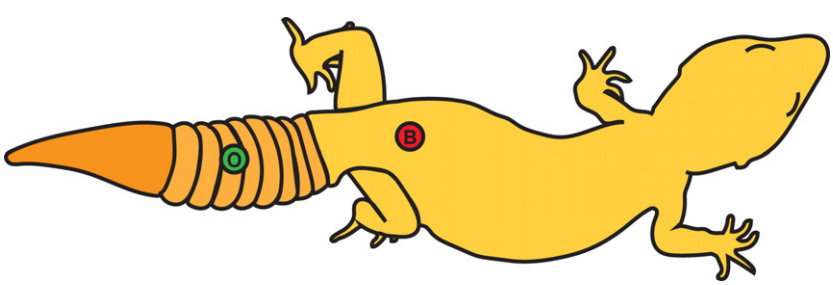

Fig. 1 Schematic of biopsy wound locations on the leopard gecko. Each animal received two full-thickness 3-mm-diameter biopsies. All biopsies were positioned slightly off the midline of the body axis. Body biopsies (B) were located 1 mm cranial to the pelvis. Original distal tail (O) biopsies were located distal to the fifth tail segmentation (autotomy plane). Twenty-four animals received body and original distal tail biopsies.

Table 1 Summary table of the optimised immunohistochemistry and immunofluorescence protocols for proteins of interest.

Antigen	Type	Retrieval	Block	Primary	Secondary	HRP	DAB
WE6	IHC	12 min citrate buffer	3% NGS 1.5 h RT	Mouse anti-WE6 1 : 5 (Developmental Studies Hybridoma Bank WE6-s)	Biotinylated goat anti-mouse 1 : 200 (Vector Laboratories BA-9200)	1 : 200	40 s
PCNA	IHC	None	3% NGS 1 h RT	Rabbit anti-PCNA 1 : 500 (Santa Cruz Biotechnology, Inc. sc-7907)	Biotinylated goat anti-rabbit 1 : 200 (Jackson ImmunoResearch Laboratories, 111-066-003)	1 : 200	25 s
VEGF	IHC	12 min citrate buffer	3% NGS 1 h RT	Rabbit anti-VEGF 1 : 100 (Santa Cruz Biotechnology, Inc. sc-152)	Biotinylated goat anti-rabbit 1 : 500 (Jackson ImmunoResearch Laboratories, 111-066-003)	1 : 200	25 s
TSP-1	IHC	12 min citrate buffer	3% NGS 1 h RT	Mouse anti-Thrombospondin 1 1 : 50 (Santa Cruz Biotechnology, sc-59887)	Biotinylated goat anti-mouse 1 : 500 (Vector Laboratories BA-9200)	1 : 200	40 s
vWF	IF	None	3% NGS 1 h RT	Rabbit anti-vonWillebrand Factor 1 : 500 (Dako Canada, A0082)	Cy3 goat anti-rabbit 1 : 400 (Jackson ImmunoResearch Laboratories, 111-165-144)		
α-SMA	IF	None	3% NGS 1 h RT	Mouse anti-α-Actin 1 : 400 (Santa Cruz Biotechnology, sc-32251)	Goat anti-mouse AlexaFluor-488 1 : 400 (Life Technologies, A-11001)		

then rinsed with three (2 min) changes of PBS and then incubated with a biotinylated secondary antibody diluted in PBS for 1 h at room temperature (for details and specific dilutions, see Table 1). Slides were then rinsed with three (2 min) changes of PBS and incubated with horseradish peroxidase-conjugated streptavidin (HRP; Jackson ImmunoResearch Laboratories, West Grove, PA, USA, code: 016-030-084) diluted in PBS for 1 h at room temperature (for specific dilutions, see Table 1). Slides were rinsed in three (2 min) changes of PBS, followed by the addition of 3,3′-diaminobenzidine peroxidase substrate (DAB; Vector Laboratories; for specific times, see Table 1). The chromogen reaction was halted by immersing the slide in deionised water. Sections were counterstained for 1 min in Mayer's haematoxylin, rinsed with deionised water, blued in ammonia water and rinsed in deionised water. Slides were dehydrated through three (2 min) changes each in 100% isopropanol and xylene. Slides were then coverslipped using Cytoseal (TM) (Fischer Scientific).

Immunofluorescence

To visualise blood vessels, double-labelled immunofluorescence, for both vonWillebrand factor (vWF; expressed by endothelial cells) and α-smooth muscle actin (α-SMA; expressed by perivascular cells), was performed. As above, slides were rehydrated to water and then rinsed with three (2 min) changes of PBS. Sections were then blocked using 3% NGS diluted in PBS for 1 h. Sections were then incubated overnight at 4 °C with primary antibodies diluted in PBS (for details and specific dilutions, see Table 1), or for the negative control sections, PBS. Slides were then rinsed with three (2 min) changes of PBS and then incubated with the secondary antibodies diluted in PBS (for details and specific dilutions, see Table 1) for 1 h at room temperature. Slides were rinsed in three (2 min) changes of PBS followed by the addition of 4′,6-diamidino-2-phenylindole (DAPI; Life Technologies D1306, Carlsbad, CA, USA) diluted 1 : 10 000 in sterile PBS (1 min). Slides were rinsed in three (2 min) changes of PBS and then coverslipped using Dako Fluorescent Mounting Medium (Dako Canada S3023, Burlington, Ontario, Canada).

Results

Original (unwounded) integument

Prior to wounding, the integument of the dorsal and lateral body and tail surfaces is characterised by a mosaic of small, similarly sized imbricating scales interspersed with a regular arrangement of larger tubercle scales. Tubercle scales are conical or dome-shaped, and approximately five times larger in diameter than the mosaic scales. Leopard geckos typically demonstrate a conspicuous pattern of countershading, with their dorsal and lateral surfaces coloured in shades of yellow and orange, with a variable series of darker grey and black spots, while their ventral surfaces are typically pale and lack spots.

At the level of histology, the epidermis is a stratified, squamous, keratinised epithelium, ranging in thickness from two to eight cell layers, depending on the phase of the shedding cycle. The underlying dermis contains pigment cells along with blood vessels, nerves and isolated inflammatory cells, and consists of both superficial and deep compartments. The superficial dermis is primarily found within the scales and consists of loose connective tissue. The deep dermis is continuous over the entire body surface and consists of dense irregular connective tissue. Deep to the dermis is the hypodermis, composed of loose connective tissue and unilocular adipocytes. Whereas it is thin across much of the body, the hypodermis becomes thicker and more adipocyte-rich along the tail.

Gross morphology of scar-free wound healing

To study the process of wound healing, 3-mm-diameter full-thickness (epidermis, dermis and into the hypodermis)

circular biopsy wounds were created in four dorsally positioned locations (two per gecko): (i) original tail; (ii) body in the region of the abdomen; (iii) base of the tail (that portion of the tail not capable of autotomy); and (iv) regenerated tail. At both 8 and 45 DPW, wounds were grossly similar at each of the four locations (Fig. S2). As such, the present study focuses on details of wound healing of the original tail (hereafter, 'tail') and body locations only (Fig. 1).

Bleeding following wounding was minimal (i.e. restricted to the wound margins, if at all), and there was no evidence of immediate wound contraction. Instead, similar to humans, the wounds remained open and healed by secondary intention. The creation of biopsy wounds had no observed effect on behaviour or growth (see Data S1), and none of the wound sites ($n = 70$) developed any evidence of infection or inflammation in any of the animals at any time during the experiment (e.g. no redness or swelling around the injury).

The gross morphological events of wound healing for both original tail and body biopsy locations were similar; hence, these data are presented together (Fig. 2; see also Fig. S1). By 0.5 DPW, each biopsy site developed a clot of blood, tissue fluid and tissue debris. The clot was lost by 8–14 DPW, revealing a smooth, unpigmented wound epithelium. Beginning from 14 DPW, pigmentation followed by the reformation of scales occurred starting from the wound margins and proceeding to the centre of the wound. At no time was granulation tissue observed. By 28 DPW, the wound epithelium was covered by small, pigmented, glassy scales. By 45 DPW, coverage by normally sized, opaque scales was fully restored. Regenerated scales were similar in size to mosaic pavement scales of the uninjured dermis, but were more irregular in both size and shape. Tubercle scales were not replaced.

Histology of scar-free wound healing

To document the tissue-level events of wound healing, serial histology was used. At each of the time points, the descriptions are begun with biopsy wounds made to the original tail, followed by a comparison with biopsy wounds made to the body. An exudate clot formed across the wound site of both tail and body wounds within 0.5 DPW. This clot was often lost during tissue processing, suggesting that adhesion of this structure to the wound bed is poor. The sections confirm that biopsies to the tail (Fig. 3A) and body (Fig. 3B) were full thickness, and in some cases involved the underlying skeletal muscle. Re-epithelialisation began within 2 DPW (Fig. 3C,D). At the tail biopsy site (Fig. 3C), the wound epithelium was composed of one to four layers of round to squamous cells. A similar histology was observed at the body biopsy sites (Fig. 3D): the wound epithelium was incomplete and one to five cell layers thick.

Re-epithelialisation was complete within 5 DPW. Deep to the new wound epithelium a collection of small, round cells

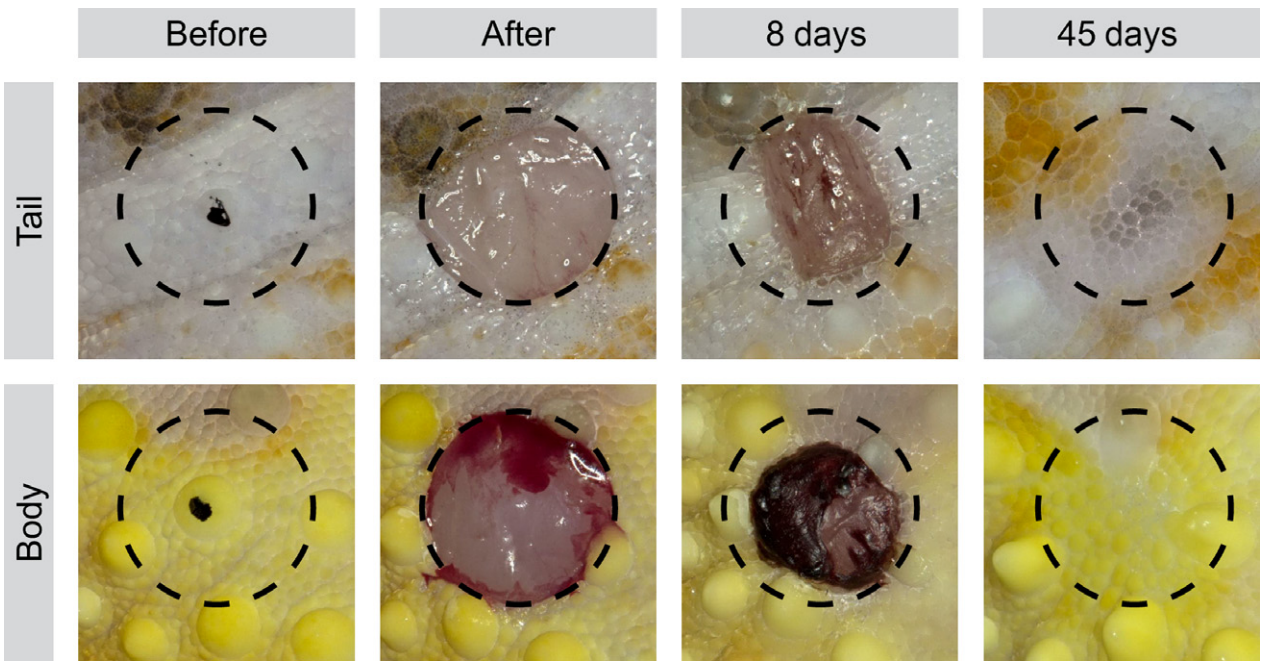

Fig. 2 Macroscopic sequence of scar-free wound healing of the tail and body of the leopard gecko. Biopsies taken from specific locations on the body and tail, each centred on a tubercle scale (black dot; before). Full-thickness excisional wounds, 3 mm in diameter, were created to remove a plug of epidermis, dermis and subdermal tissue (after). At 8 DPW, a clot capped the excisional injuries. At 45 DPW, the excised tissue was macroscopically restored and covered with a mosaic of small scales. Tubercular scales were not restored. Circle diameter = 3 mm.

began to accumulate within a loosely organised matrix (Fig. 3E,F). At first glance, this cellular matrix appeared to closely resemble the early formation of granulation tissue. However, unlike granulation tissue, this cellular matrix never becomes hypervascularised. At the tail biopsy site (Fig. 3E), the wound margins were clearly identifiable. Compared with the uninjured dermis, the newly formed cellular matrix had considerably less ECM, as indicated by blue-green staining of collagen fibres, and the wound epithelium was six to 10 cell layers thick. A similar histology was observed at the body biopsy sites (Fig. 3F). The margin between the uninjured dermis and the wound bed was distinct with very little ECM amongst the cells of the newly forming matrix. The wound epithelium was complete, six to 10 cell layers thick. Compared with tail wounds, body wound sites were more cellular, and had less ECM.

By 8 DPW, the newly formed matrix was noticeably thicker and more cell-rich compared with previous time points (Fig. 3G,H). At the tail biopsy site (Fig. 3G), the interface between the wound bed and the uninjured dermis remained discernible, although collagen deposition had begun. The wound epithelium was six–10 cell layers thick and demonstrated evidence of increasing keratinisation. Body biopsy sites had comparable histology (Fig. 3H), with a clearly distinguishable wound margin and evidence of collagen deposition. The wound epithelium of the body biopsy locations was identical to that of the tail. However, compared with tail biopsy locations, the cellular matrix of the body wounds appeared to be more densely cellular and less collagen-rich.

By 14 DPW, scale formation had begun, and the underlying cellular matrix was beginning to remodel (Fig. 3I,J). At the tail biopsy site (Fig. 3I), the wound margins were no longer clear, as the new tissue aggregating within the defects became less cellular and more collagenous. At this time point, the wound epithelium was beginning to thin (five to eight cells layers thick). The body biopsy site had similar histology (Fig. 3J), with indistinct wound margins, and increasing evidence of dense, irregularly organised collagen bundles in the wound bed. The wound epithelium was four to eight cell layers thick. At this time point, pigment cells were first observed along the epidermal–dermal interface of both tail and body wounds. Collagen organisation within the wound bed was comparatively looser in tail than body wounds, reminiscent of the collagen organisation of uninjured dermis in the two locations.

By 28 DPW, the biopsy sites closely resembled uninjured cutaneous tissues (Fig. 3K,L). At the tail biopsy site (Fig. 3K), the wound margins were indistinct and the new dermis consisted of fibroblast-like cells and loose, collagen-rich connective tissue. The wound epithelium was comparable in thickness to the original epidermis (i.e. four to six cell layers thick). As in tail wounds, the new dermis of the body wound bed consisted mainly of fibroblast-like cells within an irregularly organised collagen ECM. The wound epithelium was two to five cell layers thick. Compared with those of the tail, body wounds appeared to be more cellular and have a denser arrangement of collagen. Adipocytes were absent from the hypodermal layers of both tail and body wounds.

Tail and body wounds were completely healed by 45 DPW (Fig. 3M,N). Restoration of the epidermis and dermis was complete, such that the only evidence of the former wound bed was at the level of adipocytes within the hypodermis of tail wounds (small or absent at the wound site, large and abundant in the original; Fig. 3M). The wound margins were unidentifiable, and the new dermis was fully restored to a loose connective tissue. The thickness of the wound epithelium matched that of the original (two to six cell layers thick). Body wounds were only identifiable based on interruptions in the underlying epaxial muscle (Fig. 3N), as the wound margins were no longer perceptible. The dermis consisted of dense irregular connective tissue, and the wound epithelium was two to five cell layers thick.

Tissue events of epidermal restoration

Restoration of the epidermis began at 2 DPW, with the growth of thin tongues of epithelium from the wound edges toward the centre of the wound. This developing wound epithelium was identified using the wound keratin marker WE6 (Fig. 4A,B). Cells within all layers of the newly forming wound epithelium were positive for the proliferation marker PCNA, indicating that they are actively proliferating over the wound site, rather than simply migrating (Fig. 4C,D). By 8 DPW, the wound epithelium was hyperthickened in both tail and body wounds (Fig. 4E,F), and was intensely positive for WE6. $PCNA^+$ cells were restricted to the lower half of the epidermis (Fig. 4G,H). By 28 DPW, the wound epithelium thinned. It remained $WE6^+$ (Fig. 4I,J), and $PCNA^+$ cells were largely restricted to the basal layer of the epidermis (Fig. 4K,L).

Histology of dermal restoration

The first signs of new dermal tissue within both the tail and body biopsy sites were observed at 5 DPW, beginning with the appearance of a highly cellular aggregate beneath the wound epithelium (Fig. 5A,B). Gradually, this cell-rich tissue became increasingly invested with an irregularly organised ECM (e.g. 14 DPW; Fig. 5C,D), but at no time were any isolated α-SMA^+ myofibroblasts observed. By 45 DPW, the new dermis was completely reformed. Histologically indistinguishable from the surrounding, uninjured tissue (Fig. 5E,F), the neo-dermis includes structurally mature blood vessels (see below) and an irregular, basket-weave organisation of collagen entirely distinct from the parallel bundle architecture otherwise characteristic of scar tissue (Fig. 5G,H).

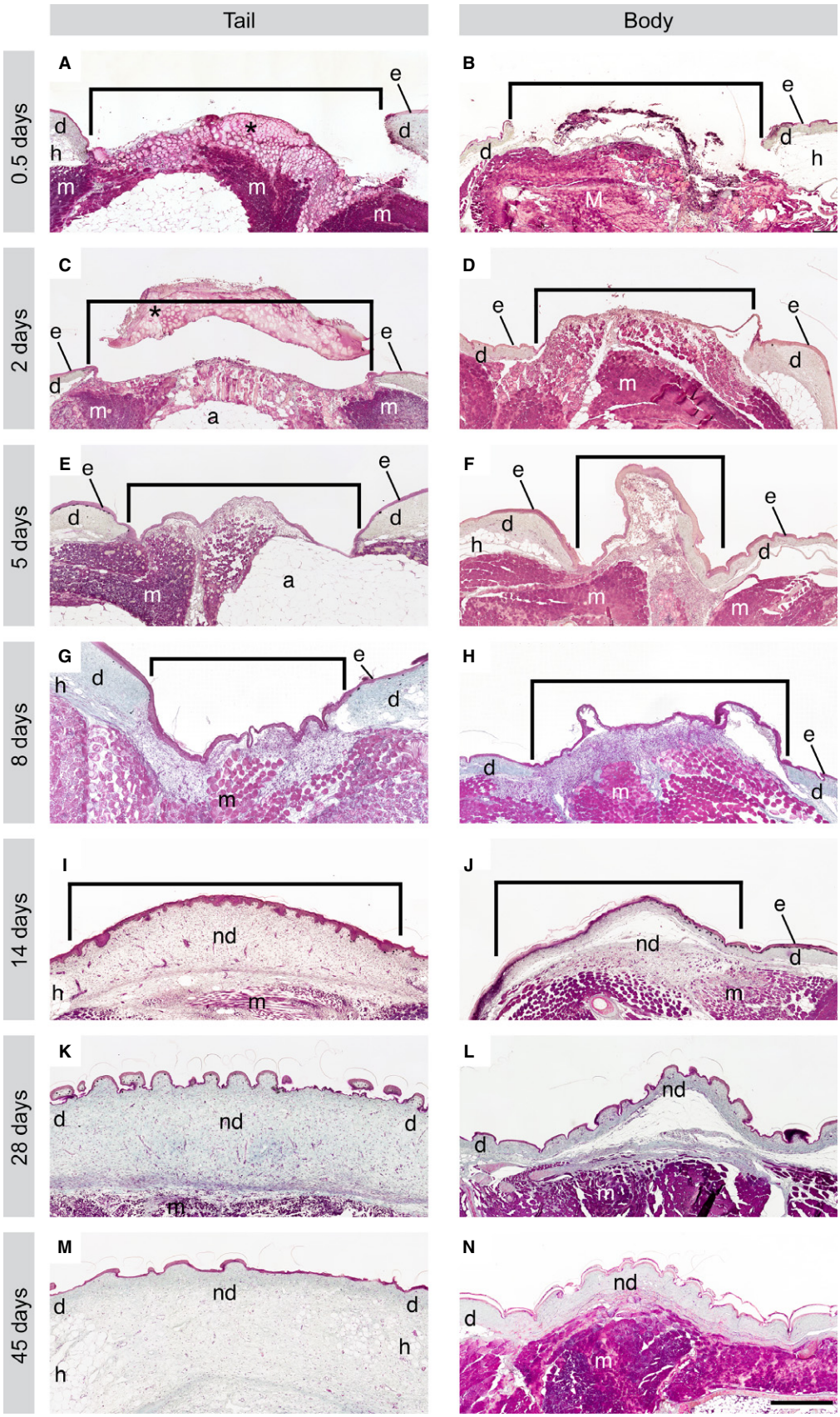

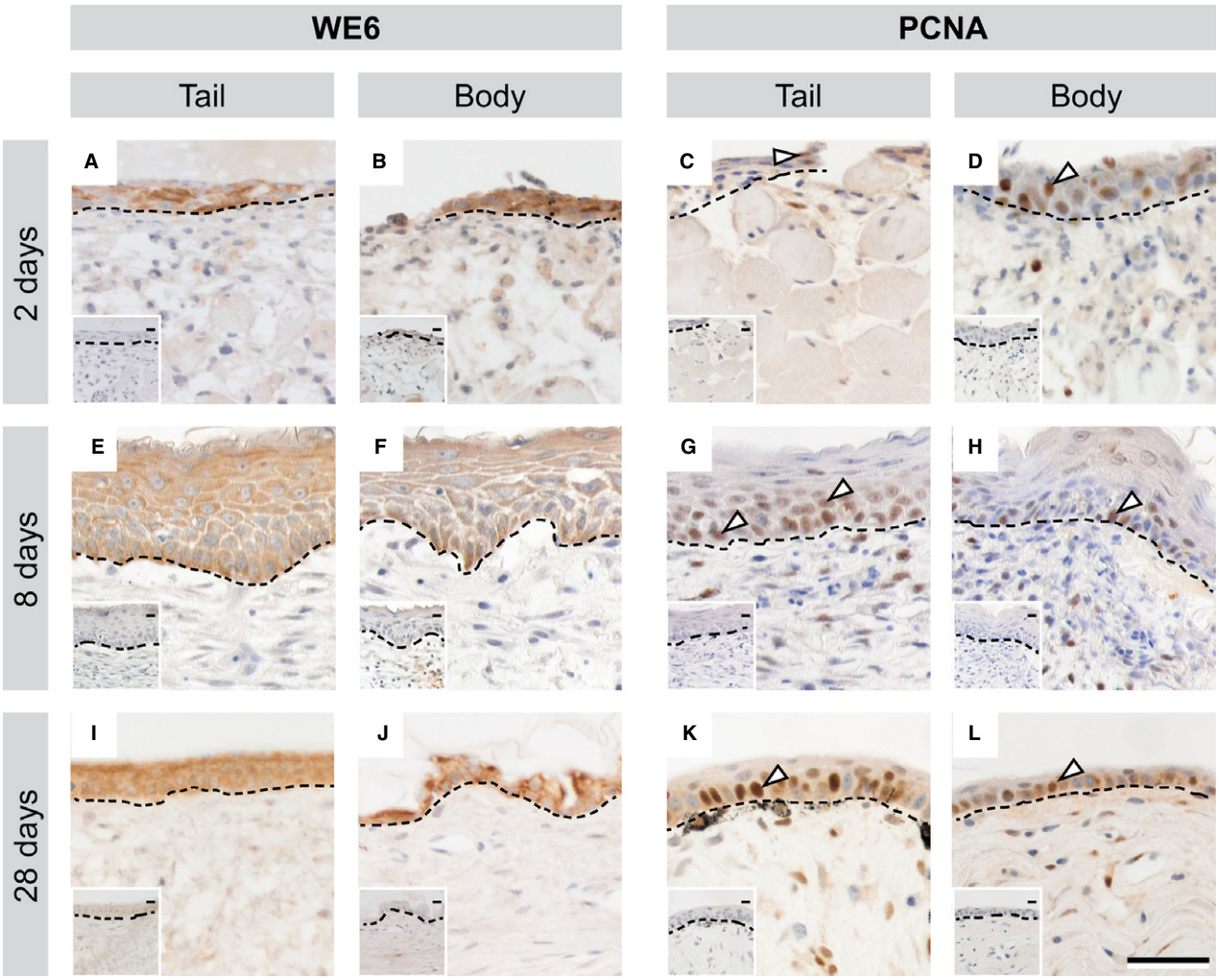

Fig. 4 Epidermal restoration began 2 DPW, and involved the formation of a multi-layered proliferative wound epithelium after cutaneous wounding in the leopard gecko. At 2 DPW, a WE6$^+$ wound epithelium began to grow from the edges of both tail and body wounds (A, B). Cells within multiple layers of the newly forming epidermis were PCNA$^+$ (C, D). By 8 DPW, the wound epithelium was hyperthickened and intensely WE6$^+$ (E, F) with PCNA$^+$ cells present in the lower layers of the epidermis (G, H). At 28 DPW, the wound epithelium had thinned, though remained WE6$^+$ (I, J), while PCNA$^+$ cells were largely restricted to the basal layer (K, L). Dashed line indicates division between epidermal (upper) and dermal (lower) tissues. White arrow indicates example PCNA$^+$ cells. Scale bar: 40 μm. Insets: negative controls with primary antibody omitted.

Revascularisation during scar-free wound healing

To characterise the vasculature of the provisional tissue, immunofluorescence for vWF was used to label endothelial cells and α-SMA to label perivascular cells (Fig. 6). The presence of α-SMA$^+$ cells intimately associated with vWF$^+$ blood vessels indicates that the blood vessels have recruited perivascular support cells (pericytes or smooth muscle cells),

Fig. 3 Wound healing was completed within 45 days, with no histological evidence of granulation tissue after cutaneous wounding in the leopard gecko. Tissue sections from both tail and body wounds were stained with Masson's trichrome. At 0.5 DPW, the wound is covered by a clot (*; A), which was often lost during processing (B). By 2 DPW, a wound epithelium was beginning to grow beneath the clot (C, D). At 5 DPW, the wound epithelium was complete and a collection of round cells began to form beneath the wound epithelium (E, F). The cellular aggregate was thickened at 8 DPW (G, H). The ECM was readily visible at 14 DPW, and undulations in the epithelium indicated the beginning of scale formation (I, J). By 28 DPW, the wound margins were nearly indiscernible, and the wound site was filled with a collagenous matrix consistent with uninjured dermis, though slightly more cell-rich in appearance (K, L). By 45 DPW, the wound site was only distinguishable in the tail by a lack of large adipocytes (M), and in the body wounds only by disruptions in underlying muscle (N). The dermis and epidermis were histologically identical. Brackets indicate wound margins. Scale bar: 500 μm. Trichr, trichrome staining; *, clot; e, epidermis; d, dermis; h, hypodermis; m, muscle; nd, new (healed) dermis.

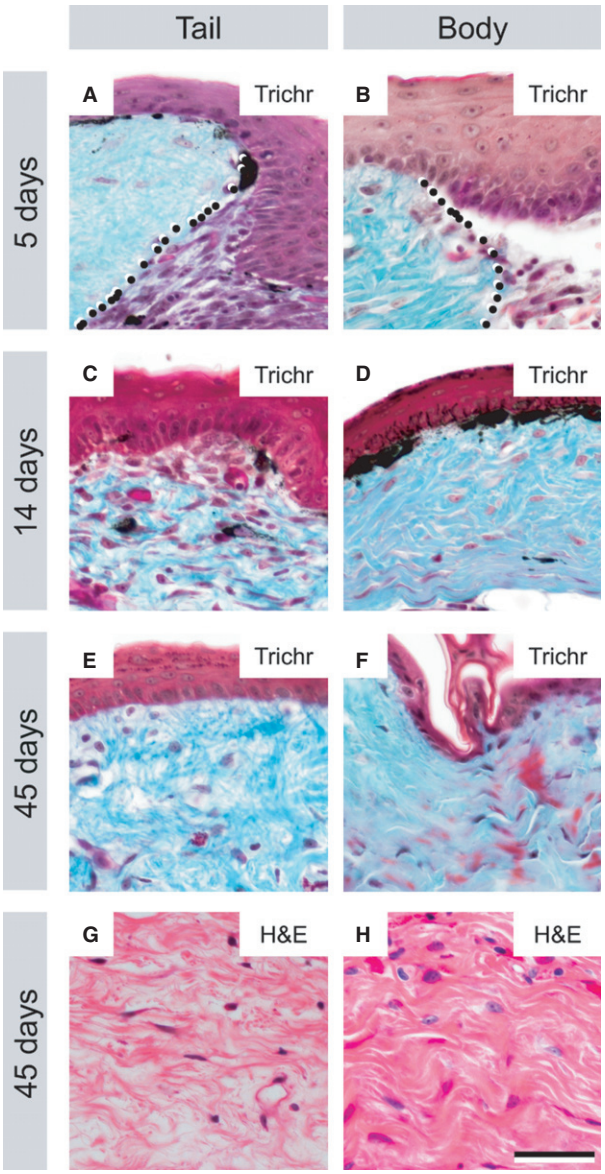

Fig. 5 Dermal repair proceeds through a cell-rich intermediate to re-form basket-weave organised tissue after cutaneous wounding in the leopard gecko. At 5 DPW, the wound margin is distinct, with a cell-rich aggregate forming beneath the wound epithelium (A, B: dotted line indicates wound margin with original dermis, left, and cell-rich aggregate in the wound bed, right). By 14 DPW, collagenous fibres (blue-green) have formed among the cells within the wound site (C, D). The new dermis becomes progressively more ECM rich, and reduces in cellularity until 45 DPW (E, F). At this time point, the ECM is organised in a basket-weave pattern characteristic of normal dermis, not parallel bundles indicative of scar formation (G, H). Scale bar: 40 μm. Trichr, trichrome staining; H&E, haematoxylin and eosin staining.

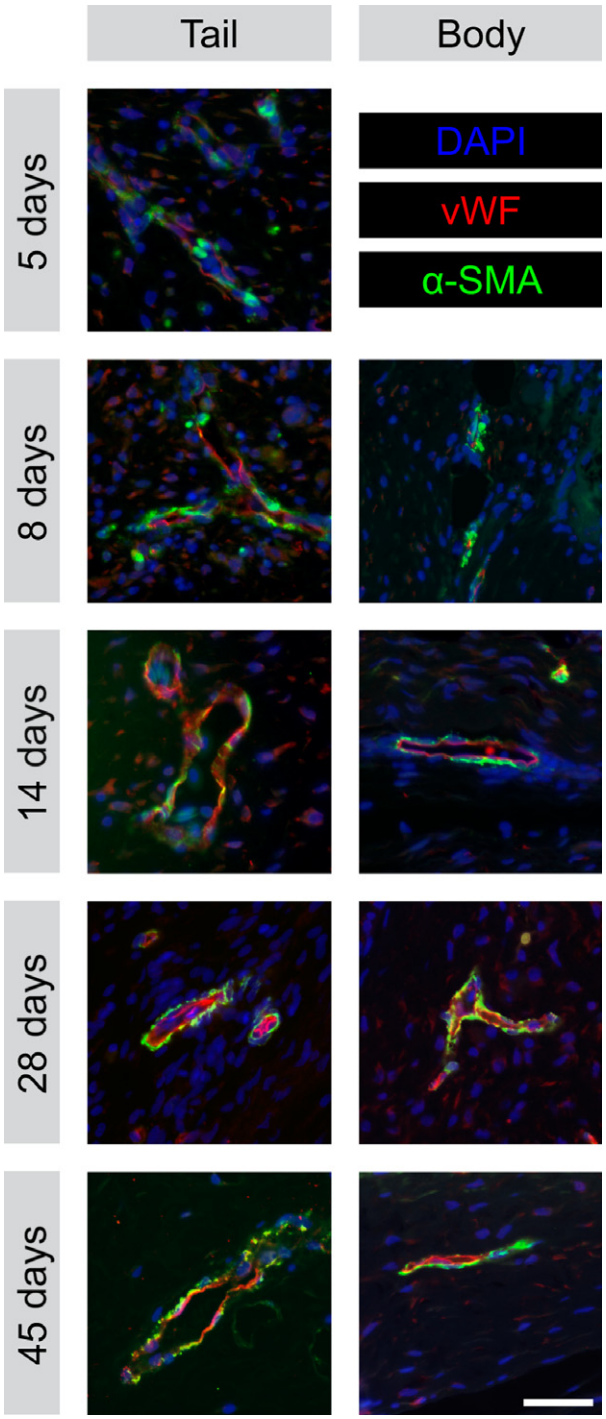

Fig. 6 Stabilised blood vessels appear 5–8 days after cutaneous wounding of the leopard gecko. Blood vessels within the wound bed of the body and original tail wounds at 5, 8, 14, 28 and 45 DPW. Endothelial cells immunostained with anti-vonWillebrand factor (vWF) and labelled with Cy3 (red). Perivascular cells immunostained with anti-α-smooth muscle actin (α-SMA) and labelled with AlexaFluor-488 (green). Nuclei counterstained with DAPI (blue). Scale bar: 40 μm.

consistent with a structurally mature vascular phenotype (Gaengel et al. 2009; Armulik et al. 2011). Blood vessels were absent in body and tail wounds prior to 5 DPW. In tail biopsy wounds at 5 DPW, occasional vWF$^+$ blood vessels were identified along the periphery of the wound bed. Notably, subsets of these early-formed vessels were already associated with α-SMA$^+$ perivascular cells. At 8 DPW, tail wounds had numerous, vWF$^+$ blood vessels with prominent,

but discontinuous association with α-SMA$^+$ perivascular cells. The first evidence of vWF$^+$ blood vessels in body wounds was observed at 8 DPW. Similar to 5 DPW tail wounds, blood vessels were only located adjacent to the wound margins, and some were associated with α-SMA$^+$ cells. By 14 DPW, both tail and body wounds were vascularised with a modest network of vWF$^+$/α-SMA$^+$ blood vessels. This mature vasculature arrangement persisted throughout subsequent time points within both the tail and body wounds. At no time did the density of these blood vessels obviously exceed that observed in the uninjured dermis (Fig. S3). To better understand these findings, the immunohistochemical expression of two potent endogenous proteins known to regulate angiogenesis was investigated: the pro-angiogenic VEGF; and the anti-angiogenic TSP-1. It was found that both VEGF and TSP-1 were widely expressed by cells of the transitional matrix of the wound bed starting at 5 DPW and continuing throughout the wound-healing process (Fig. 7).

Discussion

Full-thickness excisional wounds to the integument of leopard geckos heal without scar formation. Like many species of lizards, leopard geckos are able to spontaneously regenerate a lost tail (Bellairs & Bryant, 1985). Tail regeneration begins with a period of scar-free wound healing, followed by tissue outgrowth and differentiation. Unexpectedly, it was found that the regenerative capacity of the skin is not restricted to the regeneration-competent tail, but is also demonstrated by the integument covering the dorsal surface of body. These findings indicate that, at least in some lizards (but not all, see Wu et al. 2014), scar-free wound healing, including the restoration of scales and the basket-weave architecture of the dermis, is an intrinsic property of the integument.

Following excisional injury, wound beds had minimal bleeding and became capped by a clot within 12 h.

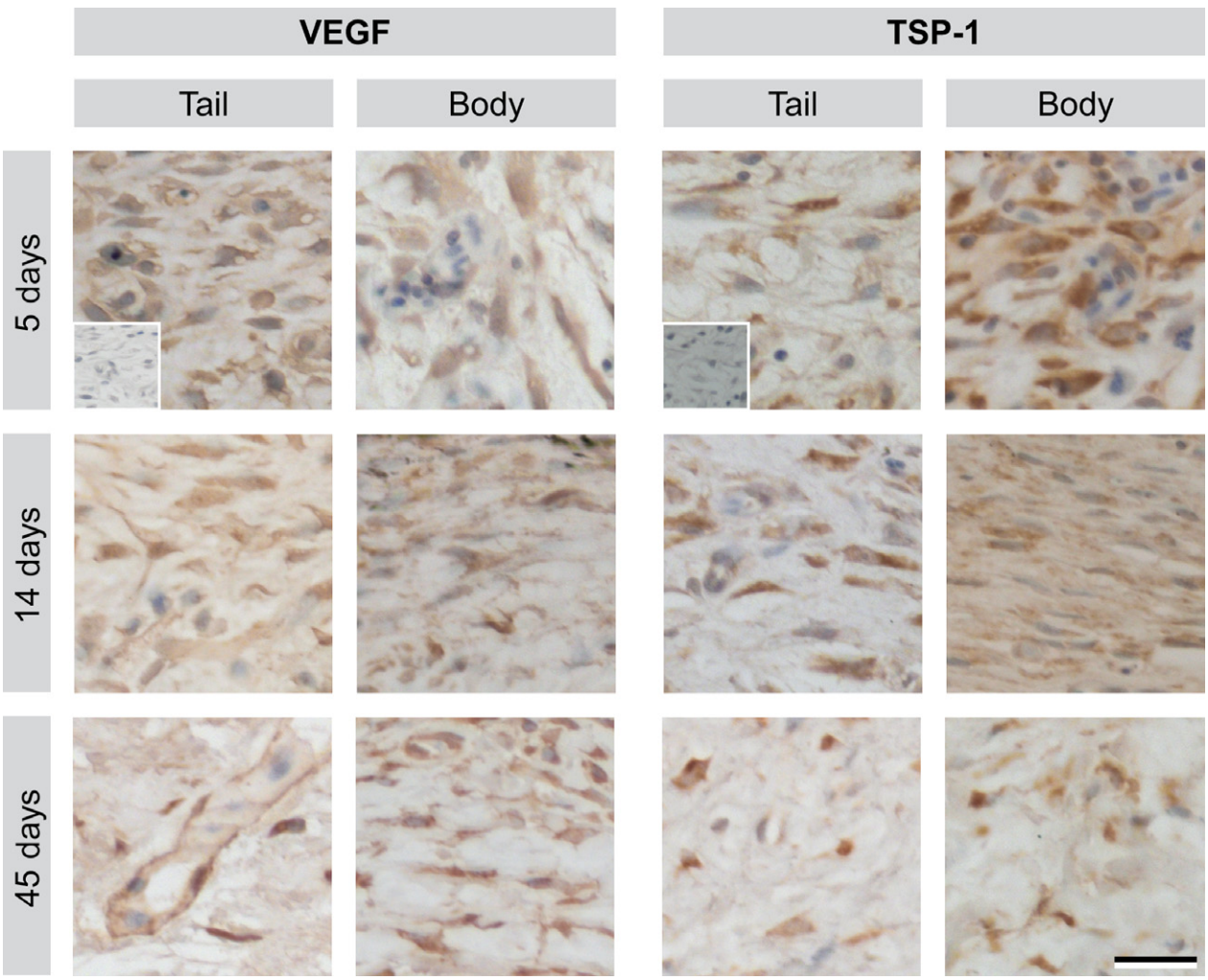

Fig. 7 Vascular endothelial growth factor A (VEGF) and thrombospondin-1 (TSP1) are expressed throughout scar-free wound healing. Immunohistochemistry for VEGF and TSP-1 within the wound matrix at 5–45 DPW following 3 mm excisional biopsy punch wounds in the tail and body. Inset: negative controls with primary antibody omitted. Scale bar: 20 μm.

Compared with reports of scarring wounds, scar-free wound healing in leopard geckos is characterised by rapid re-epithelialisation of the injury site, postponed initiation of collagen deposition within the wound bed, and a delayed and tightly regulated angiogenic response. Of particular importance, no evidence of hypervascularised granulation tissue formation was observed. Ultimately, the scar-free wound-healing program resulted in the restoration of a near-perfect integument, complete with pigmented scales and dermis. In addition, restoration of the dermis yielded a basket-weave organisation of ECM quite unlike the in-parallel arrangement observed following scar formation. While the current study was conducted on subadult leopard geckos (i.e. < 1 year old and not sexually mature), identical outcomes were observed in a reproductively mature individual of at least 4 years old (personal observations, HMP and MKV); therefore, the ability to scar-free wound heal appears to be retained well into adulthood in this species. Though not the focus of the present work, the current data indicate that the leukocytic response to the biopsy injuries is limited, involving relatively few inflammatory cells and no other obvious tissue-level hallmarks (e.g. swelling).

Wound closure occurs by secondary intention without granulation tissue formation

Cutaneous excisional wounds in the leopard gecko healed by secondary intention. Wound healing by secondary intention typically occurs following unsutured excisional injuries in humans and other tightly-skinned animals (e.g. lizards, pigs, frogs and salamanders; Christenson et al. 2005; Lévesque et al. 2010; Yokoyama et al. 2011; Seifert et al. 2012; Bertolotti et al. 2013; Chadwick et al. 2013). In contrast, mice, perhaps the most common model for the study of cutaneous wound healing, rapidly minimise the wound area by contracting the subdermal panniculus carnosus muscle (Galiano et al. 2004; Dunn et al. 2013). Consequently, to more closely model human excisional injuries, cutaneous wounds in mice must be splinted open to ensure their repair through secondary intention (Galiano et al. 2004; Dunn et al. 2013).

The wound bed becomes invested with a transitional tissue comprised largely of fibroblast-like cells. Although this tissue initially bears a resemblance to granulation tissue due to its high cellularity, numerous proliferating cells and inclusion of fibrous ECM, it lacks the otherwise defining feature of excessive vascularity. Similar fibroblast-rich granulation-like tissue has also been reported for wound healing in urodeles (Seifert et al. 2012; Seifert & Maden, 2014), although the extent of the angiogenic response remains unclear. The formation of a hypervascular granulation tissue is almost universally recognised as a mediator of scarification in mammals (Satish & Kathju, 2010; Seifert et al. 2012) and adult frogs (Bertolotti et al. 2013). Less is known about reptilian wound healing. The formation of granulation tissue followed by scarring has been documented for various non-regenerating wounds, though details of the vascular response were not reported (Mader, 2006; Alibardi, 2010). Alternatively, the common garter snake (*Thamnophis sirtalis*) has been described as forming scars without a granulation tissue intermediate (Smith & Barker, 1988).

In the leopard gecko, re-epithelialisation of 3 mm diameter biopsy wounds to both the body and original tail is completed within 5 DPW. Rapid wound epithelium closure is characteristic of other scar-free wound-healing species, including axolotls, *Xenopus laevis* froglets and African spiny mice (Lévesque et al. 2010; Yokoyama et al. 2011; Seifert et al. 2012, 2013). By comparison, similarly-sized scarring wounds require 1–2 weeks to develop a complete wound epithelium (Coulombe, 1997; Galiano et al. 2004; Lucas et al. 2010; Chen et al. 2014). One proposed role of rapid wound epithelium closure during scar-free wound healing is that it may contribute to a reduction in inflammation (Seifert et al. 2012), though molecular mechanisms supporting this observation have not been established. Combined, these data indicate that rapid wound epithelium closure is a hallmark of the scar-free wound-healing program, underscoring this process as a possible target for ongoing efforts to reduce scarring.

Scales and pigmentation are restored

As for other geckos (Noble & Bradley, 1933; Maderson, 1971), leopard geckos restore scales following cutaneous excisional wounding. Among other reptiles, the ability to regenerate scales varies. For example, in *Anolis carolinensis* excisional injuries to the tail, but not the body, re-developed scales, but neither body nor tail wounds re-established scales in *Iguana iguana* (Wu et al. 2014). In common garter snakes (*T. sirtalis*; Smith & Barker, 1988), cutaneous wounds scar and do not re-scale, whereas the regenerated tail of the Tuatara (*Sphenodon punctatus*) does re-rescale, with the exception of the distal-most 1–4 mm (Alibardi & Maderson, 2003). Among other amniotes, integumentary appendages are also redeveloped as part of the scar-free healing program (e.g. hair follicles in spiny mice), but are not restored in scarring wounds (Gurtner et al. 2008; Seifert et al. 2013). Scar-free wound healing amphibians, including axolotls and larval frogs, regenerate functional epidermal glands, while scar-forming adult frogs do not (Yannas et al. 1996; Lévesque et al. 2010; Seifert et al. 2012; Bertolotti et al. 2013). Whereas the mosaic pavement of imbricating scales is regenerated following wounding in leopard geckos, the conical-shaped tubercle scales are not. Furthermore, the overall organisation of these scales differs, due to the absence of tubercles. Similar observations have been reported for various other lizard species (Woodland, 1920; Noble & Bradley, 1933; Maderson, 1971; Wu et al. 2014). In

addition, a similar pattern of scale regeneration (i.e. mosaic scales without tubercles) also occurs following complete tail loss and regeneration (e.g. McLean & Vickaryous, 2011). Recent work has demonstrated that the *de novo* regeneration of scales is distinct from original scale development (Wu et al. 2014), which may explain why tubercles are not restored. The re-establishment of mosaic scales and the basket-weave collagen architecture of the dermis are evidence that the absence of tubercles is unrelated to scar formation.

Unlike some lizards, leopard geckos are able to restore complex pigmentation colours (e.g. yellows and oranges) during the scar-free wound-healing program. In lizards, skin colouration is provided by four chromatophores: melanophores, xanthophores, iridophores, and erythrophores (Kuriyama et al. 2006). The range of colours observed is the result of different organisations of chromatophores, with black being achieved by the exclusive presence of melanophores (Kuriyama et al. 2006). Whereas functional dermal chromatophore units are formed within the regenerating skin of leopard geckos from 14 DPW, some lizards, such as *A. carolinensis* and *I. iguana*, fail to restore the original (yellow–green) colouration, even at 45–80 DPW (Wu et al. 2014).

Dermal restoration involves delayed collagen deposition

The current findings are consistent with previous observations that scar-free wound healing is characterised by delayed onset of collagen deposition and limited to non-existent participation by myofibroblasts. By contrast, myofibroblasts are key participants in fibrosis (Darby et al. 1990; Epstein et al. 1999; Etich et al. 2013; Kramann et al. 2013), and are rapidly recruited to the wound bed following the initial phase of inflammation (Duffield et al. 2013). In addition to contraction of the defect, myofibroblasts also secrete abundant ECM, particularly parallel bundles of type I collagen (Duffield et al. 2013), as early as 3–4 DPW in scar-forming mammals (Levenson et al. 1965; Greaves et al. 2013). Whereas α-SMA$^+$ myofibroblasts are transiently present at the wound site following tail loss in leopard geckos (Delorme et al. 2012), no evidence for these cells within the biopsy wound beds was found. Related to this, deposition of irregularly organised collagen (i.e. normal dermal collagen) at the wound site was comparatively delayed; it was not initiated until 8 DPW, and only become abundant at 14 DPW. Parallel bundles of collagen characteristic of scarring were never present in the wound bed. Similarly, the absence or limited participation of α-SMA$^+$ myofibroblasts and a delayed initiation of collagen deposition has also been reported during scar-free cutaneous wound healing in African spiny mice (Seifert et al. 2013) and axolotls (Lévesque et al. 2010; Seifert et al. 2012).

Hypodermal restoration is delayed

Among geckos, the hypodermis of the tail serves as an important location of lipid storage, with well-nourished individuals developing large numbers of hypertrophic adipocytes (Russell et al. 2015). As expected, no evidence of adipocytes in healed body wounds was found, as hypodermis over the body of geckos is typically minimal. In contrast, by 45 DPW, excisional wounds to the tail showed evidence of a limited restoration of the adipocyte population. Curiously, it only takes leopard geckos 21 days fully to restore hypodermal adipose tissue during tail regeneration (Delorme et al. 2012). The reason for the difference in adipocyte restoration during cutaneous wound healing vs. tail regeneration remains uncertain; however, recent work in mice has revealed that populations of fibroblast-like cells from the reticular (deep) dermis include pre-adipocytes, and contribute to scar formation (Driskell et al. 2013). During reptilian cutaneous wound healing, fibroblasts are reported to mainly migrate from the superficial dermal layer (Maderson & Roth, 1972; Smith & Barker, 1988). As a result, the delayed adipocyte restoration in gecko cutaneous wounds may be related to a reduced contribution from the deep dermal fibroblasts.

Blood vessel formation during scar-free wound healing

In the leopard gecko, the wound bed is devoid of vasculature until 5–8 DPW. Throughout the remainder of the wound-healing program, the apparent vascular density of the newly forming tissue never appears to exceed that of the surrounding, uninjured dermis, and there is no evidence of widespread vascular regression. Furthermore, most of the blood vessels are supported by perivascular cells and can reasonably be interpreted as structurally mature. In contrast, scarring wounds of mammals and frogs are characterised by hypervascularised granulation tissue (a transitional structure composed of abundant fibroblast-like cells and a profuse, structurally immature vascular network; Gurtner et al. 2008; Bertolotti et al. 2013). The vascular density of granulation tissue peaks at 3–5 DPW (Bluff et al. 2006; Chen et al. 2014). As the tissue remodels, the once extensive vascular network gradually regresses, transforming the tissue into a permanent, hypovascular, fibrotic scar (Reinke & Sorg, 2012; Dipietro, 2013). The association between blood vessels and scar tissue is also supported by experimental studies. Impairing vascularisation of the wound bed with the use of a neutralising anti-VEGF antibody promotes a reduction in scar size and the formation of a more basket-weave collagen architecture characteristic of uninjured dermis (Wilgus et al. 2008). In contrast, the addition of exogenous VEGF promotes vascularisation and scarring in foetal wounds, which would normally heal scar-free (Wilgus et al. 2008). Hence, the quantity and quality of

blood vessels formed during wound healing appears to profoundly influence the ultimate mode of wound resolution.

The molecular mechanism responsible for the more proportionate vascular response during scar-free wound healing remains unclear. Unexpectedly, there was widespread expression of both the pro-angiogenic factor VEGF and the anti-angiogenic protein TSP-1 during scar-free wound healing. During scar formation, VEGF is widely expressed, beginning almost immediately following wounding, and promotes the disproportionate angiogenic response characteristic of granulation tissue (Barrientos et al. 2008). TSP-1 expression peaks at 3 DPW, in parallel with the maximal vascular density in granulation tissue (Dipietro et al. 1996; Agah et al. 2002; Bluff et al. 2006; Chen et al. 2014). Curiously, TSP-1-null mice do not exhibit increased granulation tissue vascularity compared with wild-type mice, suggesting that TSP-1 is not controlling re-vascularisation of scarring wounds (Agah et al. 2002). Combined, these data suggest that the expression of other pro- and anti-angiogenic factors may be involved in modulating the vascular response in wound healing.

Concluding remarks

Although cutaneous scarring and scar-free wound healing involve a comparable sequence of tissue events, there are important differences in re-epithelialisation, blood vessel formation and the ultimate organisation of collagen. The current results reveal that the excisional wound bed becomes in-filled with a cell-rich aggregation, but that this tissue never becomes hypervascularised. This proportional vascular response may be important for minimising or averting scar formation.

Acknowledgements

The authors sincerely thank H. Coates, S.L. Delorme, S.L. Payne, J. Vieira and J.J. Petrik for technical assistance and discussion, and two anonymous reviewers for improvements to the manuscript. The WE6 antibody was developed by R.A. Tassava, and was obtained from the Developmental Studies Hybridoma Bank, created by the NICHD of the NIH and maintained at The University of Iowa, Department of Biology, Iowa City, IA 52242, USA. This work was supported by a Natural Sciences and Engineering Research Council of Canada (NSERC) Discovery Grant (400358) to MKV, an Alexander Graham Bell Canada Graduate Scholarship (NSERC CGS-M) to HMP, an Ontario Graduate Scholarship to EABG, and Ontario Veterinary College Fellowships to HMP and EABG.

Authors' contributions

HMP performed the biopsies, collected and sectioned the tissue, performed the histochemistry, immunohistochemistry and immunofluorescence, and drafted the manuscript. EABG developed the anaesthesia protocol, assisted with biopsies and edited the manuscript. MKV conceived of the study, assisted with biopsies, captured the gross images and participated in writing the manuscript. All authors participated in care of the animals, and read and approved the final manuscript.

References

Agah A, Kyriakides TR, Lawler J, et al. (2002) The lack of Thrombospondin-1 (TSP1) dictates the course of wound healing in double-TSP1/TSP2-null mice. *Am J Pathol* **161**, 831–839.

Alibardi L (2010) Morphological and cellular aspects of tail and limb regeneration in lizards: a model system with implications for tissue regeneration in mammals. *Adv Anat Embryol Cell Biol* **2010**, 1–207.

Alibardi L, Maderson PFA (2003) Observations on the histochemistry and ultrastructure of regenerating caudal epidermis of the tuatara *Sphenodon punctatus* (Sphenodontida, Lepidosauria, Reptilia). *J Morphol* **256**, 134–145.

Armulik A, Genove G, Betsholtz C (2011) Pericytes: developmental, physiological, and pathological perspectives, problems, and promises. *Dev Cell* **21**, 193–215.

Barrientos S, Stojadinovic O, Golinko MS, et al. (2008) Perspective article: growth factors and cytokines in wound healing. *Wound Repair Regen* **16**, 585–601.

Baum CL, Arpey CJ (2005) Normal cutaneous wound healing: clinical correlation with cellular and molecular events. *Dermatol Surg* **31**, 674–686.

Bellairs AD, Bryant SV (1985) Autotomy and regeneration in reptiles. In: *Biology of the Reptilia* . (eds Gans C, Billett F), pp. 303–410. New York: John Wiley and Sons.

Bertolotti E, Malagoli D, Franchini A (2013) Skin wound healing in different aged *Xenopus laevis*. *J Morph* **274**, 956–964.

Bluff JE, O'Ceallaigh S, O'Kane S, et al. (2006) The microcirculation in acute murine cutaneous incisional wounds shows a spatial and temporal variation in the functionality of vessels. *Wound Repair Regen* **14**, 434–442.

Blyth E (1854) Proceedings of the Society. Report of the Curator, Zoological Department. *J Asiat Soc Bengal* **23**, 737–740.

Chadwick SL, Yip C, Ferguson MWJ, et al. (2013) Repigmentation of cutaneous scars depends on original wound type. *J Anat* **223**, 74–82.

Chen L, Mehta ND, Zhao Y, et al. (2014) Absence of CD4 or CD8 lymphocytes changes infiltration of inflammatory cells and profiles of cytokine expression in skin wounds, but does not impair healing. *Exp Dermatol* **23**, 189–194.

Christenson LJ, Phillips PK, Weaver AL, et al. (2005) Primary closure vs second-intention treatment of skin punch biopsy sites: a randomized trial. *Arch Dermatol* **141**, 1093–1099.

Clark RAF, Ghosh K, Tonnesen MG (2007) Tissue engineering for cutaneous wounds. *J Invest Dermatol* **127**, 1018–1029.

Coulombe PA (1997) Towards a molecular definition of keratinocyte activation after acute injury to stratified epithelia. *Biochem Biophys Res Commun* **236**, 231–238.

Darby I, Skalli O, Gabbiani G (1990) Alpha-smooth muscle actin is transiently expressed by myofibroblasts during experimental wound healing. *Lab Invest* **63**, 21–29.

Delorme SL, Lungu IM, Vickaryous MK (2012) Scar-free wound healing and regeneration following tail loss in the Leopard Gecko, *Eublepharis macularius*. *Anat Rec* **295**, 1575–1595.

Dipietro LA (2013) Angiogenesis and scar formation in healing wounds. *Curr Opin Rheumatol* **25**, 87–91.

Dipietro LA, Nissen NN, Gamelli RL, et al. (1996) Thrombospondin 1 synthesis and function in wound repair. *Am J Pathol* **148**, 1851–1860.

Driskell RR, Lichtenberger BM, Hoste E, et al. (2013) Distinct fibroblast lineages determine dermal architecture in skin development and repair. *Nature* **504**, 277–281.

Duffield JS, Lupher M, Thannickal VJ, et al. (2013) Host responses in tissue repair and fibrosis. *Annu Rev Pathol* **8**, 241–276.

Dunn L, Prosser HCG, Tan JTM, et al. (2013) Murine model of wound healing. *J Vis Exp* **75**, e50265–e50265.

Epstein FH, Singer AJ, Clark RA (1999) Cutaneous wound healing. *N Engl J Med* **341**, 738–746.

Etich J, Bergmeier V, Frie C, et al. (2013) PECAM1(+)/Sca1(+)/CD38(+) vascular cells transform into myofibroblast-like cells in skin wound repair. *PLoS One* **8**, e53262.

Ferguson MWJ, O'Kane S (2004) Scar-free healing: from embryonic mechanisms to adult therapeutic intervention. *Philos Trans R Soc Lond B Biol Sci* **359**, 839–850.

Ferguson MWJ, Whitby DJ, Shah M, et al. (1996) Scar formation: the spectral nature of fetal and adult wound repair. *Plast Reconstr Surg* **97**, 854–860.

Gaengel K, Genove G, Armulik A, et al. (2009) Endothelial-mural cell signaling in vascular development and angiogenesis. *Arterioscler Thromb Vasc Biol* **29**, 630–638.

Galiano RD, Michaels J, Dobryansky M, et al. (2004) Quantitative and reproducible murine model of excisional wound healing. *Wound Repair Regen* **12**, 485–492.

Greaves NS, Ashcroft KJ, Baguneid M, et al. (2013) Current understanding of molecular and cellular mechanisms in fibroplasia and angiogenesis during acute wound healing. *J Dermatol Sci* **72**, 206–217.

Guo S, DiPietro LA (2010) Factors affecting wound healing. *J Dent Res* **89**, 219–229.

Gurtner GC, Werner S, Barrandon Y, et al. (2008) Wound repair and regeneration. *Nature* **453**, 314–321.

Kramann R, DiRocco DP, Humphreys BD (2013) Understanding the origin, activation and regulation of matrix-producing myofibroblasts for treatment of fibrotic disease. *J Pathol* **231**, 273–289.

Kuriyama T, Miyaji K, Sugimoto M, et al. (2006) Ultrastructure of the dermal chromatophores in a lizard (Scincidae: *Plestiodon latiscutatus*) with conspicuous body and tail coloration. *Zoolog Sci* **23**, 793–799.

Levenson SM, Geever EF, Crowley LV, et al. (1965) The healing of rat skin wounds. *Ann Surg* **161**, 293–308.

Lévesque M, Villiard E, Roy S (2010) Skin wound healing in axolotls: a scarless process. *J Exp Zool B Mol Dev Evol* **314**, 684–697.

Lorenz HP, Longaker MT, Perkocha LA, et al. (1992) Scarless wound repair: a human fetal skin model. *Development* **114**, 253–259.

Lucas T, Waisman A, Ranjan R, et al. (2010) Differential roles of macrophages in diverse phases of skin repair. *J Immunol* **184**, 3964–3977.

Mader DR (2006) Abscesses. In: *Reptile Medicine and Surgery* . (ed. Mader DR), pp. 715–719. Philadelphia: Saunders.

Maderson PFA (1971) The regeneration of caudal epidermal specializations in *Lygodactylus picturatus keniensis* (Gekkonidae, Lacertilia). *J Morphol* **134**, 467–477.

Maderson PFA, Roth SI (1972) A histological study of the early stages of cutaneous wound healing in lizards *in vivo* and *in vitro*. *J Exp Zool* **180**, 175–185.

Martin P, D'Souza D, Martin J, et al. (2003) Wound healing in the PU.1 null mouse-tissue repair is not dependent on inflammatory cells. *Curr Biol* **13**, 1122–1128.

McLean KE, Vickaryous MK (2011) A novel amniote model of epimorphic regeneration: the leopard gecko, *Eublepharis macularius*. *BMC Dev Biol* **11**, 50.

Noble GK, Bradley HT (1933) The effect of temperature on the scale form of regenerated lizard skin. *J Exp Zool* **65**, 1–16.

Occleston NL, Metcalfe AD, Boanas A, et al. (2010) Therapeutic improvement of scarring: mechanisms of scarless and scar-forming healing and approaches to the discovery of new treatments. *Dermatol Res Pract* **2010**, 1–10.

Pyron RA, Burbrink FT, Wiens JJ (2013) A phylogeny and revised classification of Squamata, including 4161 species of lizards and snakes. *BMC Evol Biol* **13**, 93.

Reinke JM, Sorg H (2012) Wound repair and regeneration. *Eur Surg Res* **49**, 35–43.

Ross MH, Pawlina W (2011) *Histology: A Text and Atlas*, 6th edn. Philadelphia: Lippincott Williams & Wilkins.

Russell AP, Lynn SE, Powell GL, et al. (2015) The regenerated tail of juvenile leopard geckos (Gekkota: Eublepharidae: *Eublepharis macularius*) preferentially stores more fat than the original. *Zoology* **118**, 183–191.

Satish L, Kathju S (2010) Cellular and molecular characteristics of scarless versus fibrotic wound healing. *Dermatol Res Pract* **2010**, 790234.

Schumacher J, Yelen T (2006) Anesthesia and analgesia. In: *Reptile Medicine and Surgery* . (ed. Mader DR), pp. 442–452. Philadelphia: Saunders.

Seifert AW, Maden M (2014) New insights into skin regeneration. *Int Rev Cell Mol Biol* **310**, 129–169.

Seifert AW, Monaghan JR, Voss SR, et al. (2012) Skin regeneration in adult axolotls: a blueprint for scar-free healing in vertebrates. *PLoS One* **7**, e32875.

Seifert AW, Kiama SG, Seifert MG, et al. (2013) Skin shedding and tissue regeneration in African spiny mice (*Acomys*). *Nature* **489**, 561–565.

Smith DA, Barker IK (1988) Healing of cutaneous wounds in the common garter snake (*Thamnophis sirtalis*). *Can J Vet Res* **52**, 111–119.

Vickaryous MK, McLean KE (2011) Reptile Embryology. In: *Methods in Molecular Biology* . (ed. Pelegri FJ), pp. 439–455. Totowa: Humana Press.

Wilgus TA, Ferreira AM, Oberyszyn TM, et al. (2008) Regulation of scar formation by vascular endothelial growth factor. *Lab Invest* **88**, 579–590.

Woodland W (1920) Some observations on caudal autotomy and regeneration in the gecko (*Hemidactylus flaviviridis,* Rüppel), with notes on the tails of Sphenodon and Pygopus. *Q J Microsc Sci* **65**, 63–100.

Wu P, Alibardi L, Chuong C-M (2014) Regeneration of reptilian scales after wounding: neogenesis, regional difference, and molecular modules. *Regeneration (Oxford)* **1**, 15–26.

Yannas IV, Colt J, Wai YC (1996) Wound contraction and scar synthesis during development of the amphibian *Rana catesbeiana*. *Wound Repair Regen* **4**, 29–39.

Yates CC, Hebda P, Wells A (2013) Skin wound healing and scarring: fetal wounds and regenerative restitution. *Birth Defects Res C* **96**, 325–333.

Yokoyama H, Maruoka T, Aruga A (2011) Prx-1 expression in *Xenopus laevis* scarless skin-wound healing and its resemblance to epimorphic regeneration. *J Invest Dermatol* **131**, 2477–2485.

Supporting Information

Additional Supporting Information may be found in the online version of this article:

Data S1. Body weight measurements for animals in biopsy study.
Fig. S1. Scar-free cutaneous excisional wound healing in the tail and body of leopard geckos, *Eublepharis macularius*.
Fig. S2. Scar-free cutaneous excisional wound healing at various locations on the leopard gecko, *Eublepharis macularius*.
Fig. S3. Blood vessels in the unwounded dermis and wound matrix in the leopard gecko, *Eublepharis macularius*.